A Systematic Methodology for Kinetic Modeling of Chemical Reactions Applied to *n*-Hexane Hydroisomerization

Kenneth Toch, Joris W. Thybaut, and Guy B. Marin
Laboratory for Chemical Technology, Ghent University, Ghent B-9052, Belgium

DOI 10.1002/aic.14680
Published online November 22, 2014 in Wiley Online Library (wileyonlinelibrary.com)

Kinetic modeling provides chemical engineers with a unique opportunity to better understand reaction kinetics in general and the underlying chemistry in particular. How to systematically approach a modeling assignment in chemical reaction kinetics is typically less clear, especially for novices in the field. The proposed modeling methodology pursues an adequate compromise between statistical significance and physical meaning of the kinetic model and the corresponding parameters and typically results in models of an appropriate complexity. It comprises the following activities: (1) data analysis, aiming at qualitative information on the reaction mechanism and corresponding rate equations, (2) model regression to quantify this information via optimal parameter values, and (3) validation of the statistical significance and physical meaning of the parameter estimates. This methodology is successfully applied to n-hexane hydroisomerization on a bifunctional catalyst. © 2014 American Institute of Chemical Engineers *AIChE J*, 61: 880–892, 2015
Keywords: kinetic modeling, systematic approach, n-*hexane, hydroisomerization, bifunctional zeolite*

Introduction

Among other aspects, chemical reaction and reactor engineering focuses on the development of comprehensive models, accounting for net production rates based on intrinsic chemical kinetics as well as for transport phenomena at the catalyst pellet and the reactor scale.[1,2] Reactor integration into an overall plant and the corresponding optimization heavily rely on adequate reactor and kinetic models which should, hence, be an essential element in the toolbox mastered by chemical engineers. Adopting a systematic methodology offers strategic advantages for chemical engineers when constructing such a model. This leads to an increased understanding of the occurring phenomena and facilitates academic and industrial communication between researchers in a similar field.

Chemical engineering requires a multiscale approach in which kinetics are situated centrally between the fundamental phenomena occurring at the catalyst scale and the applied phenomena at the reactor scale. Kinetic modeling bridges the gap between these two by the integration of experimentally observed reaction rates and first principles into a kinetic model. Excellent reference works on this topic was written by Kittrell[3] and Dumesic.[4] Depending on the purpose of the kinetic model, a certain degree of detail is needed. For example, a simple power law or a Langmuir–Hinshelwood/Hougen–Watson model may suffice for simulating industrial reactor behavior in the vicinity of a stable operating point. If a better understanding of the reaction mechanism is aimed at, enabling rational catalyst design and multiscale reactor optimization, more complex, microkinetic models are necessary. The construction of such more detailed, microkinetic models, requires more detailed information about the kinetics which may be obtained via specific experimental techniques and test units, for example, temporal analysis of products and gravimetric microbalance reactors.[5,6]

This work is focused on establishing this systematic methodology for the kinetic modeling of thermal and catalytic chemical reactions from experimental kinetic data, resulting in adequate kinetic models with a sound physical meaning and a statistical significance. The acquisition of intrinsic kinetic data, that is, in the absence of transport limitations, both mass and heat, should be the main goal when an experimental campaign is designed.[7] Such transport limitations may conceal and bias the experimental observations, making the modeling of these data much more challenging. More importantly, the occurrence of such limitations would require additional adjustable model parameters in the simulation model, which potentially jeopardizes the sound statistical significance and physical meaning of the regression. For industrial reactor modeling purposes, the required transport phenomena can always be accounted for a posteriori via the proper correlations.[1] In the case of catalytic reactions, deactivation phenomena may also have to be accounted for. Intrinsic kinetics are preferentially acquired on catalysts exhibiting a long-term stability. When deactivation cannot be avoided, extrapolation can be made to time-on-stream equal to zero for the determination of initial kinetics. Specific deactivation kinetics can be determined from the time-on-stream profiles, and require dedicated modeling efforts.[8–12]

As an example through this work, a model reaction involving a limited reaction network and an established

Additional Supporting Information may be found in the online version of this article.

Correspondence concerning this article should be addressed to J. W. Thybaut at Joris.Thybaut@UGent.be.

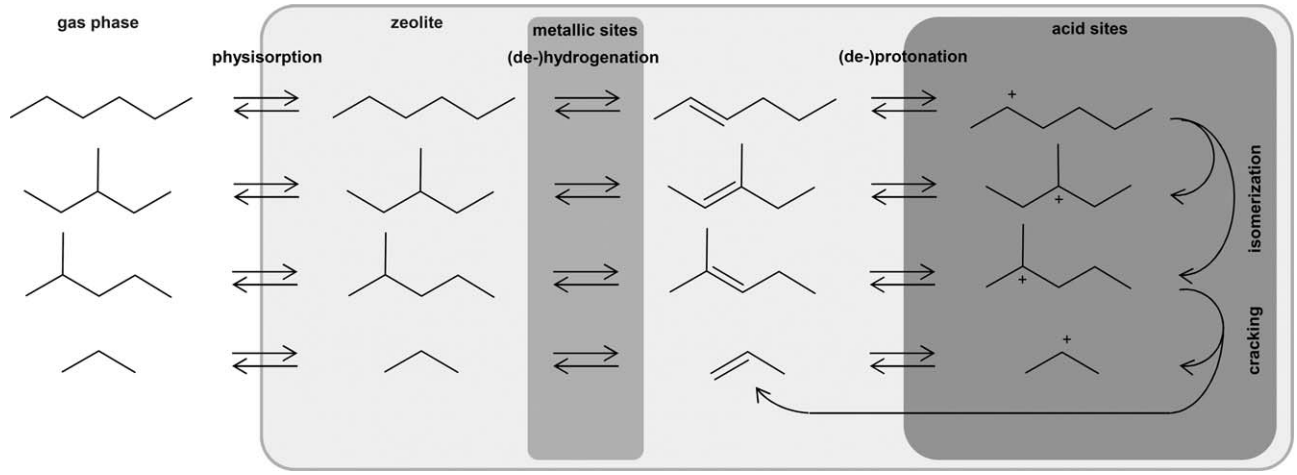

Figure 1. Schematic overview of (ideal) hydroisomerization of *n*-hexane over a bifunctional zeolite.

reaction mechanism is considered: *n*-hexane hydroisomerization over a bifunctional zeolite, that is, a with platinum impregnated H-ZSM-5 catalyst.[13–19] While the acid function provided by the H-ZSM-5 zeolite framework provokes the skeletal rearrangement and cracking, the metal function enables operating at relatively low temperatures and avoiding deactivation by coking. To acquire the most details as possible about the acid catalyzed reaction mechanism, the experimental investigation was performed at gas phase conditions under which ideal hydrocracking occurs.[15,17,18,20–24] When performing experiments within such a range of operating conditions, the acid catalyzed reactions are rate determining, leading to specific kinetic behavior, for example, exhibiting a maximum isomer yield. The hydroisomerization reaction mechanism has already been discussed extensively in literature.[21,25] A short recapitulation is given in Figure 1. In a first step, gas phase alkanes are physically adsorbed within the catalyst pores where they are subsequently dehydrogenated at the metal, that is, platinum, sites. The produced alkenes desorb from the metal sites and diffuse toward the acid sites where they are protonated to form reactive carbenium ions. These carbenium ions undergo isomerization and cracking reactions. The product carbenium ions are converted into the corresponding, observable gas phase alkanes via the sequence of elementary steps described earlier in the reverse sense.

Procedures

Experimental

Catalyst. A Pt/H-ZSM-5 catalyst was synthesized according a literature reported recipe.[26] Table 1 gives an overview of its most relevant properties. Prior to the experimentation, the catalyst was reduced *in situ* under flowing hydrogen at atmospheric pressure and 673 K during at least 4 h.

Experimental Conditions and Reactor Setup. The temperature and total pressure ranged from 493 to 573 K and 1.0–2.0 MPa with a molar inlet hydrogen to hydrocarbon ratio amounting from 50 to 100 mol mol^{-1} at a space-time of 191.0 kg_{cat} s mol_{C6}^{-1}. These reaction conditions were chosen such that intrinsic kinetics were measured.[27] External diffusion limitations were absent with the corresponding efficiency exceeding 0.998. The Weisz-Prater criterion to determine internal diffusion limitations was only narrowly satisfied with a corresponding efficiency close to 0.95. Taking into account possible diffusion effects was beyond the scope of this work due to its complexity but probably decreased the adequacy of the resulting model. Temperature gradients, both at reactor and catalyst pellet scale, were always below 0.5 K. All partial pressures were sufficiently below the corresponding vapor pressures which ensured that no condensation occurred. Also, it was experimentally verified that ideal hydrocracking occurred[15,17,18,21,23,24], see *n*-Hexane Hydroisomerization: Experimental Observations section. During experimentation, catalyst deactivation was not observed. For the complete experimental dataset, a single catalyst batch of 4.88 g was used. In total, 36 experiments were performed at 24 unique sets of experimental conditions, see Table 6 in Supporting Information.

The experiments were performed in a Berty reactor, which is a gas-phase continuous stirred tank reactor (CSTR). Prior to entering the reactor, *n*-hexane and hydrogen are mixed in an evaporator/preheater to ensure that the reactor feed is completely gaseous. The *n*-hexane flow rate is verified by monitoring the mass of the feed reservoir. After the reactor outlet, methane is added as an internal standard for analytical purposes. After reaching steady state operation after about 1 h, a sample is taken via a six-way valve and is injected on a HP Series II 5890 instrument with a 50 m (id = 0.25 mm) RSL-150 column with a 0.25 μm poly(dimethylsiloxane) film and a flame ionization detector for gas chromatography (GC). More details on the Berty reactor and setup can be found in literature.[17,18,28] After data acquisition, the experimental data are normalized making use of the carbon balance.

Definition and Calculation of Quantities and Responses. The *n*-hexane conversion, X_{nC6}, is defined as the fraction that has disappeared by reaction and is calculated as follows

Table 1. Properties of the Pt/H-ZSM-5 Catalyst

Pt Content (wt %)	$C_{H^+_{tot}}$ (mol kg_{cat}^{-1})	Si/Al-Ratio	Surface Area (10^{-3} m^2 kg^{-1})	V_p (10^{-3} m^3 kg_{cat}^{-1})
0.98	0.120	137	467	0.182

$$X_{nC6}=\frac{F^0_{nC6}-F_{nC6}}{F^0_{nC6}} \tag{1}$$

With F^0_{nC6} and F_{nC6} representing the inlet and outlet molar flow rate of *n*-hexane.

In this work, the selectivity, toward component *j* from *n*-hexane at a given conversion, is based on a carbon balance and is defined as

$$S_j=\frac{a_{C,j}}{6}\frac{F_j}{F^0_{nC6}-F_{nC6}} \tag{2}$$

with F_j the molar outlet flow rate of component *j* and $a_{C,j}$ the number of carbon atoms in component *j*.

Modeling

Reactor Model. For modeling purposes, the reactor is considered as an ideal CSTR in which no gradients nor transient behavior is observed, see Experimental Conditions and Reactor Setup section. The CSTR is described by a set of algebraic equations for the components in the reaction mixture

$$F_i=F^0_i+R_iW \qquad i=\text{2MP, 3MP, and } C_3 \tag{3}$$

with W the catalyst mass and R_i the net rate of formation of component *i*, see Eqs. 17–19. To eliminate any linear dependence in the set of reactor balance equations, the hydrogen and carbon balances were used to calculate the hydrogen and *n*-hexane molar flow rate, see resp. Eqs. 4 and 5.

$$F_{H_2}=F^0_{H_2}-\frac{F_{C3}}{2} \tag{4}$$

$$F_{nC6}=F^0_{nC6}-F_{2MP}-F_{3MP}-\frac{F_{C3}}{2} \tag{5}$$

Parameter Estimation. The regression was performed with a commercially available software package, that is, Athena Visual Studio.[29,30] In this software package, Bayesian estimation is conventionally used for multiresponse regression purposes.[31] Differences amounting to least one order of magnitude occur between the responses. Via Bayesian estimation, it is statistically assured that every response, and even each measurement within a response, is equally accounted for. The assumptions made within this package lead to an optimization criterion which is equivalent to generalized least squares. In this work, three responses are considered: the molar outlet flow rate of the products: 2-methyl pentane (2MP), 3-methyl pentane (3MP), and propane (C_3). Not including the *n*-hexane outlet flow rate as a response in the sum of squares does not bias the regression results. As the experimental data were normalized, the residuals related to *n*-hexane are linearly related to those of the other responses.

Isothermal vs. nonisothermal regression. When performing a regression, the goal is to determine the set of optimal parameters corresponding to the global extremum of the objective function. In many cases, the objective function also contains several local extrema. It is possible that, by choosing a certain set of initial parameter values, the final set of parameters obtained from regression are situated in a local extremum. Sometimes, this will not be evident from the model performance as it may seem to be adequate. This is more likely the case in highly nonlinear models, for example, when using the Arrhenius or van 't Hoff relation for describing the temperature dependency of a rate or equilibrium coefficient.

If sufficient isothermal kinetic data, that is, a subset of kinetic data in which the temperature is not varied, are available, a regression per temperature to the experimental data can be performed also denoted as isothermal regressions. This has several advantages. First, per rate coefficient only one parameter is estimated instead of two, that is, the rate coefficient itself, rather than the pre-exponential factor and the reaction enthalpy or activation energy. Second, the regression of an isothermal model which can be linearized, results in a linear regression for which a priori no initial estimates are required. By performing the isothermal regression, a value for each rate and/or equilibrium coefficient is obtained at every temperature. The coefficients obtained at every temperature can then be used to construct so-called Arrhenius and van 't Hoff plots displaying the logarithm of the concerned coefficients as a function of the inverse of the temperature.

Linear regression of these isothermally determined parameter estimates yields a value for the slope and intercept which are a measure for resp. the activation energy or reaction enthalpy and pre-exponential factor, see Eq. 6

$$\sum_{i=1}^{n_{par}}\left(k_i-A\exp\left(-\frac{E_a}{RT}\right)\right)^2 \xrightarrow{A,E_a} \text{Min} \tag{6}$$

These values typically serve as initial parameter values in the nonisothermal regression in which all data are simultaneously assessed and where the Arrhenius and van 't Hoff relationships are directly implemented. This last regression is typically considered to be the actual one as the parameters are estimated based on the minimization of the residual sum of squares of the directly observed values, see Eq. 7

$$\sum_{i=1}^{n_{exp}}\left(F_i-\hat{F}_i\right)^2 \xrightarrow{A,E_a} \text{Min} \tag{7}$$

This is the only regression which is supposed to allow determining the global extremum of the objective function; however, the above described procedure starting with isothermal regressions provides the most suitable initial guesses for this nonisothermal regression.

Reparameterization of the Arrhenius and van 't Hoff relation. The parameters in the original Arrhenius relationship, that is, the pre-exponential factor and activation energy, are typically subject to a pronounced correlation. To overcome the corresponding regression issues, reparameterized versions of these relations[3] are used in which the rate coefficient at mean temperature occurs rather than the preexponential factor, see Eq. 8. A similar reparameterization can be performed on equilibrium coefficients

$$k=k_{T_m}\cdot\exp\left(-\frac{E_a}{R}\left(\frac{1}{T}-\frac{1}{T_m}\right)\right) \tag{8}$$

Model and Parameter Estimates Assessment. The global significance of the model is typically verified by testing the null hypothesis that all parameters would simultaneously be equal to zero, via an F test.[30,32] In this F test, the ratio of the mean regression sum of squares and the mean residual sum of squares is taken, see Eq. 9

$$F_s=\frac{\frac{SSQ_{REG}}{d.f._{REG}}}{\frac{SSQ_{RES}}{d.f._{RES}}}=\frac{\frac{\sum_{i=1}^{n_{resp}}\sum_{j=1}^{n_{exp}}\hat{y}^2_{i,j}}{n_{par}}}{\frac{\sum_{i=1}^{n_{resp}}\sum_{j=1}^{n_{exp}}\left(y_{i,j}-\hat{y}_{i,j}\right)^2}{n_{exp}n_{resp}-n_{par}}} \tag{9}$$

If the calculated value exceeds the tabulated F value at a selected confidence level, for example, 95%, with the corresponding degrees of freedom, the null hypothesis is rejected and the model is deemed to be significant. In practice, the aforementioned null hypothesis is easily rejected, and, hence, for having a reliable assessment of the global significance of the model, the calculated F values should at the very least be of the order of magnitude of 100.

The model's adequacy is assessed by evaluating if the deviation between the experimental observations and model prediction can be attributed solely to experimental errors and not to a lack-of-fit of the model. If a lack-of-fit is present, systematic deviations between the model calculated and observed values occur. The model's adequacy is determined by partitioning the residuals' sum of squares, that is, the difference between model calculated and observed values, into a pure-error sum of squares, SSQ_{PE}, as determined by repeat experiments, and a lack-of-fit sum of squares, SSQ_{LOF}[3]

$$SSQ_{RES} = SSQ_{LOF} + SSQ_{PE} \tag{10}$$

The pure-error sum of squares is determined by repeat experiments as follows

$$SSQ_{PE} = \sum_{i=1}^{k} \sum_{j=1}^{n_{resp}} \sum_{l=1}^{n_e(i)} \left(y_{j,l}^{(i)} - \overline{y}_j^{(i)} \right)^2 \tag{11}$$

with k the number of different sets of repeat experiments, $n_e(i)$ the number of repeat experiments at the ith set of repeat experiments, $y_{j,l}^{(i)}$ the ith experimental observation corresponding to the ith set of repeat experiments, and the jth response and $\overline{y}_j^{(i)}$ the average value of the ith set of repeat experiments and the jth response. The corresponding degrees of freedom are given by

$$\text{d.f.}_{PE} = n_{resp} \sum_{i=1}^{k} (n_e(i) - 1) \tag{12}$$

The ratio of the lack-of-fit and pure-error sum of squares follows an F distribution with the corresponding degrees of freedom under the hypothesis that the model is adequate, see Eq. 13.

$$F_a = \frac{\frac{SSQ_{LOF}}{\text{d.f.}_{LOF}}}{\frac{SSQ_{PE}}{\text{d.f.}_{PE}}} \tag{13}$$

If the calculated F value exceeds the corresponding tabulated F value, the model is not adequate. It is evident from practice that this test is very difficult to pass, particularly for models that are nonlinear in the parameters, in contrast to the test for the global significance of the model.

The significance of every individual parameter is tested by means of a t test. In most cases, the value against which a parameter estimate is tested is zero. It is, hence, tested, if the confidence interval comprises the zero value or not. The t value is calculated by the ratio of the parameter value and its standard deviation $s(b_i)$

$$t(b_i) = \frac{b_i}{s(b_i)} \tag{14}$$

If the calculated value exceeds the tabulated value at a selected confidence level, for example, 95%, with $n_{exp}.n_{resp} - n_{par}$ degrees of freedom, the parameter is considered to be significantly different from zero. In practice, good t values are in the order of 10–100.

The binary correlation coefficient between two parameters i and j is calculated via the (co)variances of these parameters, $V(b)$, see Eq. 15. Two parameters i and j are strongly correlated if $|\rho_{i,j}| \geq 0.95$

$$\rho_{i,j} = \frac{V(b)_{i,j}}{\sqrt{V(b)_{i,i} V(b)_{j,j}}} \tag{15}$$

Besides a statistical assessment of the model and the parameter estimates, the physical significance of both should be evaluated. The physical meaning of the model is reflected in the qualitative prediction of the effect of changing reaction conditions. Additionally, the model should not result in physically unrealistic predictions. The physical meaning of the individual parameter estimates can be determined by validating if the order of magnitude of the parameter value and its sign are acceptable. If needed, literature reported values can assist in this.

Residual Analysis. The performance of a model can be assessed using statistical tests such as the F test for adequacy if based on the experimental error obtained from repetition experiments. Another method is to perform a residual analysis. This is a general term in which, among others, the following tools can be included: parity diagrams, performance figures, residual figures, and normal probability figures. Parity diagrams and performance figures allow for a visual assessment of the model's adequacy. Residual and normal probability figures, and into lesser extent parity diagrams, can be used to determine the error distribution and the occurrence of systematic deviations. A more elaborated discussion on these tools can be found in Supporting Information.

A Systematic Modeling Methodology

The kinetic modeling of chemical reactions requires the combination of different fields of expertise, for example, optimization theory,[33] parameter estimation[31] and chemical reactor, and reaction engineering.[1,2] Several authors have reported general techniques and methodologies for this purpose. For example, several methods for multiresponse parameter estimation by applying Bayesian theory[34–36] or least squares are reported.[32] The reformulation and analysis of kinetic models, including the handling of outliers, model discrimination, and experimental design is extensively discussed.[37–39] With the increased use of computers in the course of previous decades, a number of regression software packages were specifically developed for chemical kinetics modeling.[30,40,41] While all literature cited excels in describing these techniques, no work has been found which combines these techniques in an applied manner from data processing to an adequate kinetic model.

In this section, a systematic methodology for chemical kinetics modeling is proposed. It aims at maximizing the amount of information that can be retrieved while minimizing the effort. The model that is most closely corresponding to the physical reality is likely to be much more complex than the statistically most relevant model. It is important to acquire a good balance between what is physically meaningful and statistically required. The parameters obtained from regression should have a clear physical meaning with confidence intervals of an acceptable size, that is, at least inferior to the parameter value itself.[42] Also, the model adequacy should be verified to evaluate the extent to which the model

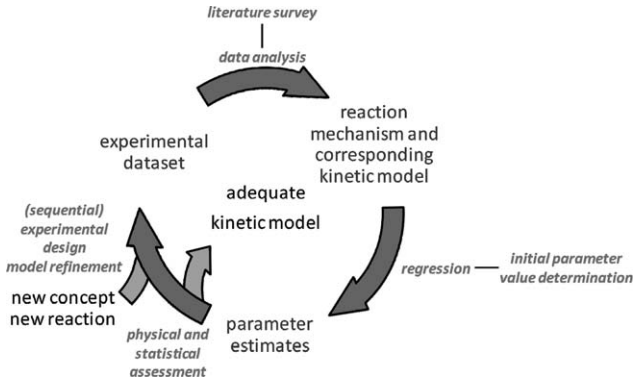

Figure 2. Systematic kinetic modeling flow diagram.

simulations deviate systematically from the experimental observations.

The methodology comprises three main steps after having acquired the experimental data: data analysis, regression, and a physical and statistical assessment, see Figure 2. Model discrimination and sequential experimental design are potential add-ons that are not further addressed in this work.

Data analysis and model construction

Prior to setting up a kinetic model, experimental data are needed which contain the necessary information to construct a kinetic model and to determine the corresponding kinetic parameters, see Figure 2.

One option to extract the valuable information from the experimental data is to plot the dependent variables, for example, molar outlet flow rates, conversions, selectivities, as function of the independent variables such as reaction temperature, inlet partial pressures, and space-time. The observed trend as function of the independent variables can then be used to evaluate apparently required functional relationships and corresponding potential reaction mechanisms.[37]

A more specific option for information extraction is to apply the method of initial rates.[1] Several kinetic models may be proposed based on different rate-determining steps, for example, adsorption, desorption, or surface reaction. Within the method of initial rates, differential experimental data which are data obtained at conversion and space-time close to zero, are plotted against the independent variables, more particularly the reactant partial pressure or the total pressure. The trend obtained is compared to that exhibited by the different methods which can lead to an initial model discrimination. Other so-called intrinsic parameter methods are also reported in literature.[43]

As indicated by Figure 2, from the knowledge gained by data analysis and literature, a reaction network and mechanism can be constructed, and the corresponding rate-equations are derived. In case of complex mixtures, pseudo components[8,44] or reaction families[45] can be defined to reduce the number of rate equations and/or model parameters.

Regression

After the data analysis and model construction, the model(s) can be regressed to the experimental data. However, due to the typical nonlinear character of kinetic models, it is important to have good initial guesses for the parameter estimates. If the initial guesses for the parameter estimates are too remote from the real values, the optimization routine might end up in a local extremum. Good initial parameter values can be obtained by linearization of the model, for example, through an isothermal regression or by a literature survey or *ab initio* calculations.[19]

During regression, typically a residual sum of squares is minimized or a probability density function is maximized. The objective function should be carefully defined in accordance with the problem formulation and may require the introduction of weights.[38] To identify the optimum of the objective function, various optimization routines are available in literature such as the Rosenbrock[46] and Levenberg–Marquardt algorithms.[47]

Physical and statistical assessment

Having performed the regression, the model performance and corresponding parameters, should be evaluated, see Figure 2. These tests are twofold: assessing the physical meaning and verifying statistical significance.

For the model, the physical meaning and statistical significance can be assessed by analyzing the residuals, as described in Residual Analysis section and Supporting Information. The parity diagram and residual and normal probability figure are mostly used to determine the statistical significance while the performance figure is used to assess the physical meaning of the model. Additionally, statistical tests can be performed for global significance of the model and model adequacy, see Model and Parameter Estimates Assessment section.

For the kinetic parameters, also both the physical meaning and statistical significance should be investigated. The first can be done by verifying if the value obtained makes physically sense, for example, the reaction order estimated is sensible, the activation energy obtained has a positive value, etc. The latter is assessed by the confidence interval of the parameter estimate, which should not include zero. If so, this parameter is deemed to be statistically insignificant and could be excluded from the kinetic model. However, the exclusion of a parameter could lead to a decrease in physical meaning as this parameter may describe intermediate steps and may diminish the extrapolatability of the kinetic model.

All these assessments can be used to determine any shortcomings in the model, which may be, but not limited to, missing reaction steps or whether the set of parameter values obtained is only a local optimum. Therefore, the kinetic model can be reformulated based on the assessment or additional experiments can be performed, preferentially via sequential experimental design, see Figure 2. If both the physical and statistical significance are fulfilled and, hence, no additions or corrections to the model are necessary, the procedure is stopped and modeling finalized.

n-Hexane Hydroisomerization: Experimental Observations

In the entire range of operating conditions, so-called ideal hydrocracking behavior was observed.[15,17,18,20–24] With increasing temperature from 493 to 573 K, the *n*-hexane conversion increased with the temperature, from about 20% to 80%, see Figure 3. A higher inlet hydrogen to *n*-hexane molar ratio and/or total pressure resulted in a decrease of the conversion, see Figure 3. If the hydrogenation reaction is in quasi-equilibrium and the inlet hydrogen to *n*-hexane molar ratio and/or total pressure increases, this equilibrium is shifted toward the alkanes, and, hence, less *n*-hexane is converted.[21]

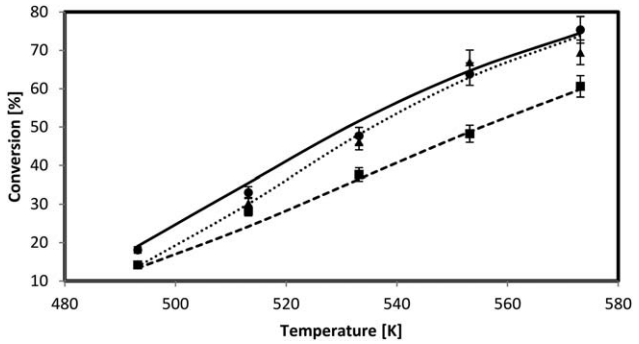

Figure 3. *n*-Hexane hydroisomerization conversion on Pt/H-ZSM-5 catalyst as a function of the temperature at different hydrogen to *n*-hexane molar inlet ratio and total pressures. Symbols correspond to experimental observations, lines correspond to model simulations, that is, Eqs. 3–5, in which the net rates of formation are given by Eqs. 17–19 using the parameters from Table 4. Filled circle, full line: $F^0_{H2}/F^0_{C6} = 50$ mol mol^{-1}, $p_{tot} = 1.0$ MPa; filled square, dashed line: $F^0_{H2}/F^0_{C6} = 100$ mol mol^{-1}, $p_{tot} = 1.0$ MPa; filled triangle, dotted line: $F^0_{H2}/F^0_{C6} = 50$ mol mol^{-1}, $p_{tot} = 2.0$ MPa.

In Figure 4, the product selectivity as function of the *n*-hexane conversion is given. At low conversions, almost exclusively isomerization via protonated cyclopropyl (PCP) branching occurs to 2MP and 3MP. In general, the ratio of 2MP and 3MP is close to 2 at *n*-hexane conversions below 50% conversion after which it decreases to the thermodynamic equilibrium around 1.5, see Figure 5. Based on the number of potential reaction pathways, the molar ratio of 2MP to 3MP expected according to kinetic considerations is one. The higher molar ratio of 2MP to 3MP than expected from this kinetic consideration can be attributed to the occurrence of intracrystalline diffusion effects[48] the latter also being confirmed by the absence of dibranched components. The critical diameter of 2MP amounts to 0.54 nm[49] and is slightly smaller than that of 3MP, that is, 0.56 nm.[48] This difference in critical diameter and spatial structure can

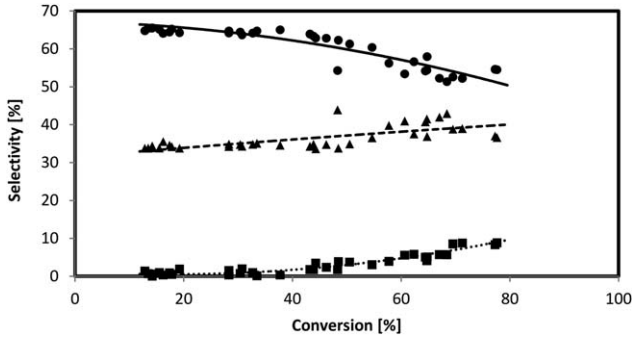

Figure 4. *n*-Hexane hydroisomerization product selectivity on Pt/H-ZSM-5 catalyst as a function of the conversion. Symbols correspond to experimental observations, lines correspond to model simulations, that is, Eqs. 3–5, in which the net rates of formation are given by Eqs. 17–19 using the parameters from Table 4. Filled circle, full line: 2MP; filled square, dashed line: 3MP; filled triangle, dotted line: propane.

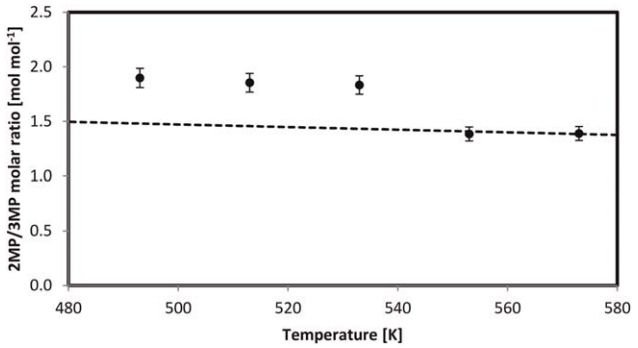

Figure 5. Molar ratio of 2MP to 3MP as function of temperature on Pt/H-ZSM-5 catalyst. The dotted line represents the calculated thermodynamic equilibrium.

indeed lead to a difference in diffusivity in the medium sized pores of the ZSM-5 zeolite investigated in this work.[48]

With increasing conversion, the relative importance of cracking via β-scission increases, as seen by the increasing propane yield, up to 8%, see Figure 4. This also results in a decrease of 2MP selectivity in favor of propane, as, the latter can only be formed from 2MP and not from 3MP according to the classical carbenium ion chemistry.

n-Hexane Hydroisomerization: Kinetic Model Development

Reaction network and catalytic cycle

In this section, a reaction network for *n*-hexane hydrocracking on a bifunctional catalyst is proposed based on the experimental observations and the corresponding catalytic cycle is constructed. Within the scope of this work, intracrystalline diffusion is not explicitly accounted for.

First, the global reaction network is constructed, see Figure 6. Experimentally, three products are observed: 2MP, 3MP, and propane. Mechanistically, 2MP and 3MP can be formed from hexane via PCP-branching, resp. via $r_{PCP(1)}$ and $r_{PCP(2)}$ in a single catalytic cycle. Propane formation from 2MP via r_{cr} is the only cracking route in hexane hydroconversion which does not involve a primary carbenium ion and, hence, the only one which occurs to an appreciable extent under the reaction conditions applied.

As an alternative, the following reaction scheme could also proposed for the hydroisomerization of *n*-hexane on Pt/H-ZSM-5, see Figure 7. For this reaction scheme, it is assumed that the reaction rate of PCP-branching of *n*-hexane toward 2MP and 3MP is equal, that is, r_{PCP}. This is justified by the same transition state through which the formation of 2MP and 3MP by PCP-branching is occurring. To account for the difference between the conversion to 2MP and 3MP,

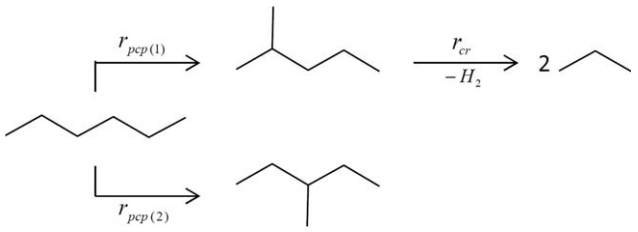

Figure 6. Simplified reaction scheme of *n*-hexane hydroisomerization on a bifunctional catalyst.

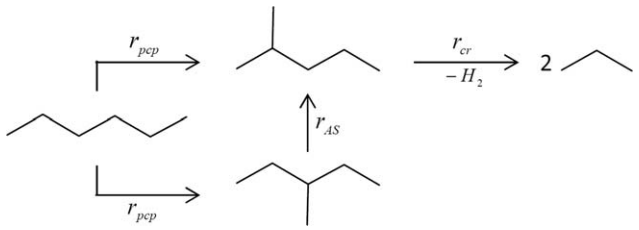

Figure 7. Alternative reaction scheme of *n*-hexane hydroisomerization on a bifunctional catalyst.

an additional isomerization step from 3MP to 2MP via an alkylshift is assumed, that is, r_{AS}.

The F values for the global significance of the model and model adequacy obtained after regression applying the alternative reaction scheme shown in Figure 7, amounted to resp. 1920 and 2.27. These values correspond both with a globally less significant and less adequate model compared to the model corresponding with the reaction scheme shown in Figure 6, also see *n*-Hexane Hydroisomerization: Modeling section. The alkylshift rate coefficient was estimated to be almost three orders of magnitude larger than the one for PCP-branching. This very fast isomerization from 3MP to 2MP compensates for the identical rate coefficients used for 2MP and 3MP formation through PCP-branching in the simulation of the experimentally observed higher 2MP production. The composite activation energy for alkylshift was estimated at -30 kJ mol^{-1}. This corresponds to an actual activation energy amounting to 30 kJ mol^{-1} for the elementary step, see Nonisothermal Regression section, which is far lower than literature reported values, that is, 80–100 kJ mol^{-1}.[19,25] Additionally, the normal probability figures indicated that the residuals were not normally distributed, see Figure 8. Hence, the alternative reaction scheme was no longer considered in favor of the kinetic model corresponding with the reaction scheme shown in Figure 6.

These values indicate a less significant and adequate model compared to the model corresponding with the reaction scheme shown in Figure 6, also see Nonisothermal Regression section. The activation energy for the alkylshift was estimated to be -33.1 kJ mol^{-1} which rather correspond a reaction enthalpy than an activation energy. Additionally, the normal probability figures indicated that the residuals were not normally distributed, see Figure 8. Hence, the alternative reaction scheme was dropped in favor of the kinetic model corresponding with the reaction scheme shown in Figure 6 and is not discussed further in this work.

The net rate of formation of all the components, that is, *n*-hexane, 2MP, 3MP, propane, and hydrogen is obtained from the rate of the individual reactions by accounting for the stoichiometry in the global reaction network, see Figure 6

$$R_{nC_6} = -r_{\mathrm{PCP}(1)} - r_{\mathrm{PCP}(2)} \tag{16}$$

$$R_{2\mathrm{MP}} = r_{\mathrm{PCP}(1)} - r_{\mathrm{cr}} \tag{17}$$

$$R_{3\mathrm{MP}} = r_{\mathrm{PCP}(2)} \tag{18}$$

$$R_{C_3} = 2r_{\mathrm{cr}} \tag{19}$$

$$R_{\mathrm{H}_2} = -r_{\mathrm{cr}} \tag{20}$$

Experimentally, the *n*-hexane conversion decreased with increasing total pressure and inlet hydrogen to *n*-hexane molar ratio, see *n*-Hexane Hydroisomerization: Experimental Observations section. As aforementioned, this is indicative of the occurrence of ideal hydrocracking. The derivation of the corresponding rate equations for the elementary steps have been described by Thybaut et al.[50]

$$r_{\mathrm{PCP}(1)} = \frac{K_{\mathrm{phys}} K_{\mathrm{deh},nC_6} K_{\mathrm{pr},nC_6} k_{\mathrm{PCP}(1)} C_{H^+_{\mathrm{tot}}} C^{\mathrm{phys}}_{\mathrm{tot}} \frac{p_{nC_6}}{p_{\mathrm{H}_2}}}{1 + K_{\mathrm{phys}}(p_{nC_6} + p_{2\mathrm{MP}} + p_{3\mathrm{MP}})} \tag{21}$$

$$r_{\mathrm{PCP}(2)} = \frac{K_{\mathrm{phys}} K_{\mathrm{deh},nC_6} K_{\mathrm{pr},nC_6} k_{\mathrm{PCP}(2)} C_{H^+_{\mathrm{tot}}} C^{\mathrm{phys}}_{\mathrm{tot}} \frac{p_{nC_6}}{p_{\mathrm{H}_2}}}{1 + K_{\mathrm{phys}}(p_{nC_6} + p_{2\mathrm{MP}} + p_{3\mathrm{MP}})} \tag{22}$$

$$r_{\mathrm{cr}} = \frac{K_{\mathrm{phys}} K_{\mathrm{deh,2MP}} K_{\mathrm{pr,2MP}} k_{\mathrm{cr}} C_{H^+_{\mathrm{tot}}} C^{\mathrm{phys}}_{\mathrm{tot}} \frac{p_{2\mathrm{MP}}}{p_{\mathrm{H}_2}}}{1 + K_{\mathrm{phys}}(p_{nC_6} + p_{2\mathrm{MP}} + p_{3\mathrm{MP}})} \tag{23}$$

With K_{phys} the physisorption equilibrium coefficient, K_{deh} the dehydrogenation equilibrium coefficient, K_{pr} the protonation equilibrium coefficient, k the rate coefficient of the elementary step, $C_{H^+_{\mathrm{tot}}}$ the total acid site concentration, $C^{\mathrm{phys}}_{\mathrm{tot}}$ the total physisorption site concentration, and p_i the partial pressure of component i. A product of several parameters occurs in the numerator of these rate expressions. To avoid a pronounced correlation between these parameters, they are lumped into a single, composite rate coefficient

$$K_{\mathrm{phys}} K_{\mathrm{deh},nC_6} K_{\mathrm{pr},nC_6} k_{\mathrm{PCP}(1)} C_{H^+_{\mathrm{tot}}} C^{\mathrm{phys}}_{\mathrm{tot}} = k^{\mathrm{comp}}_{\mathrm{PCP}(1)} \tag{24}$$

$$K_{\mathrm{phys}} K_{\mathrm{deh},nC_6} K_{\mathrm{pr},nC_6} k_{\mathrm{PCP}(2)} C_{H^+_{\mathrm{tot}}} C^{\mathrm{phys}}_{\mathrm{tot}} = k^{\mathrm{comp}}_{\mathrm{PCP}(2)} \tag{25}$$

$$K_{\mathrm{phys}} K_{\mathrm{deh,2MP}} K_{\mathrm{pr,2MP}} k_{\mathrm{cr}} C_{H^+_{\mathrm{tot}}} C^{\mathrm{phys}}_{\mathrm{tot}} = k^{\mathrm{comp}}_{\mathrm{cr}} \tag{26}$$

Of course, it may be possible to assess the catalyst descriptors such as $C_{H^+_{\mathrm{tot}}}$ and $C^{\mathrm{phys}}_{\mathrm{tot}}$ via separate, dedicated measurements. It is, however, beyond the scope of the present work aiming at a systematic methodology to further elaborate on this, and, hence, these descriptors are incorporated into the lumped rate coefficients. The final rate expressions used in the modeling of the *n*-hexane hydroconversion kinetics in terms of adjustable parameters, $k^{\mathrm{comp}}_{\mathrm{PCP}(1)}$, $k^{\mathrm{comp}}_{\mathrm{PCP}(2)}$, $k^{\mathrm{comp}}_{\mathrm{cr}}$, and K_{phys}, hence, become

$$r_{\mathrm{PCP}(1)} = \frac{k^{\mathrm{comp}}_{\mathrm{PCP}(1)} \frac{p_{nC_6}}{p_{\mathrm{H}_2}}}{1 + K_{\mathrm{phys}}(p_{nC_6} + p_{2\mathrm{MP}} + p_{3\mathrm{MP}})} \tag{27}$$

$$r_{\mathrm{PCP}(2)} = \frac{k^{\mathrm{comp}}_{\mathrm{PCP}(2)} \frac{p_{nC_6}}{p_{\mathrm{H}_2}}}{1 + K_{\mathrm{phys}}(p_{nC_6} + p_{2\mathrm{MP}} + p_{3\mathrm{MP}})} \tag{28}$$

$$r_{\mathrm{cr}} = \frac{k^{\mathrm{comp}}_{\mathrm{cr}} \frac{p_{2\mathrm{MP}}}{p_{\mathrm{H}_2}}}{1 + K_{\mathrm{phys}}(p_{nC_6} + p_{2\mathrm{MP}} + p_{3\mathrm{MP}})} \tag{29}$$

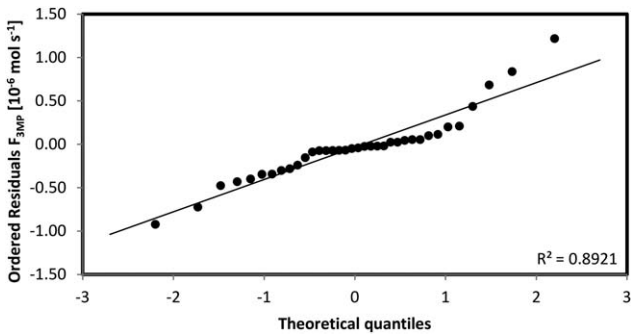

Figure 8. Normal probability figure for the molar outlet flow rate of 3MP as obtained after regression of the kinetic model corresponding with the alternative reaction scheme shown in Figure 7.

Table 2. Parameter Estimates and Corresponding 95% Confidence Interval as Function of Temperature Determined by Isothermal Regression to the Experimental Data, See Table 6 in Supporting Information, of the Kinetic Model Given by the Set of Eqs. 3–5, in Which the Net Rates of Formation are Given by Eqs. 17–19

Temperature (K)	493	513	533	553	573
$k^{comp}_{PCP(1)}$ (10^{-6} mol s^{-1} kg^{-1}_{cat})	72.9 ± 11.8	150.6 ± 40.8	215.8 ± 51.3	281.1 ± 48.7	566.9 ± 158.9
$k^{comp}_{PCP(2)}$ (10^{-6} mol s^{-1} kg^{-1}_{cat})	37.9 ± 6.4	80.2 ± 22.8	113.1 ± 28.2	189.2 ± 33.5	358.5 ± 101.9
k^{comp}_{cr} (10^{-6} mol s^{-1} kg^{-1}_{cat})	*8.9 ± 8.9*	*8.4 ± 12.9*	17.9 ± 9.0	23.6 ± 6.3	52.1 ± 16.0
K_{phys} (10^{-5} Pa^{-1})	4.0 ± 1.3	2.8 ± 2.0	*1.2 ± 1.4*	*-0.2 ± 0.7*	*1.1 ± 1.6*
F_s	676.8 (4.3)	264.3 (4.6)	327.3 (4.5)	506.9 (4.5)	283.1 (4.5)
Number of data points	9	6	7	7	7

Not statistically significant parameters are indicated in italics.

From these reaction rates, the net rate of formation of all the components, that is, *n*-hexane, 2MP, 3MP, propane, and hydrogen can be determined using Eqs. 16–20.

n-Hexane Hydroisomerization: Modeling

Isothermal regression

An isothermal regression at each of the investigated temperatures tested has been performed and yielded the estimates for the four rate coefficients, that is, $k^{comp}_{PCP(1)}$, $k^{comp}_{PCP(2)}$, k^{comp}_{cr}, and K_{phys} and the corresponding individual 95% confidence intervals as reported in Table 2.

The PCP-branching rate coefficients increase with the temperature while the ratio of both rate coefficients, $\frac{k^{comp}_{PCP(1)}}{k^{comp}_{PCP(2)}}$, decreases from about 2.0 to 1.5 with increasing temperature from 493 to 573 K. This indicates that the composite activation energy of $k^{comp}_{PCP(1)}$ is smaller than that of $k^{comp}_{PCP(2)}$. Both catalytic cycles include the same elementary steps in which a secondary carbenium ion undergoes PCP-branching leading to another secondary carbenium ion and, hence, it could be expected that the activation energies are identical. Intracrystalline diffusion phenomena are considered to be at the origin of this deviation, as explained in *n*-Hexane Hydroisomerization: Experimental Observations section. With increasing conversion, especially at higher temperatures, 2MP and 3MP are produced in amounts corresponding to thermodynamic equilibrium. Hence, the rate coefficient of PCP-branching toward 3MP has to increase faster with the temperature than that leading to 2MP, resulting in a higher activation energy of the former.

The limited cracking at lower temperatures leads to a difficult determination of the corresponding rate coefficient. As a result, its value is sometimes not significantly estimated, that is, the confidence interval includes zero as a possible parameter value. However, with increasing temperature, cracking becomes more important and, hence, the corresponding rate coefficient, k^{comp}_{cr}, increases and can be estimated significantly from 533 K onward.

The opposite holds true for the physisorption equilibrium coefficient K_{phys}. Physisorption is an exothermic step and, hence, it is most pronounced at lower temperatures. As a result, also the corresponding physisorption coefficient is statistically most significantly determined in the lower temperature range which is evident from the higher *t* values (not shown) and the corresponding relatively more narrow confidence intervals. At higher temperatures, the physisorption equilibrium coefficient adopts such a small value that in the adsorption term in Eqs. 27–29, $K_{phys}(p_{nC_6}+p_{2MeC_5}+p_{3MeC_5})$ becomes negligible compared to one and it becomes impossible to estimate the physisorption coefficient significantly.

Plotting the logarithm of the estimates for the composite rate coefficients against the reciprocal of temperature results in an Arrhenius plot, see Figure 9. For the Arrhenius plot, also the statistically nonsignificant estimates have been included as long as their value was physically meaningful. The slope of the trend lines, corresponding to $\frac{E_a}{R}$ or $\frac{-\Delta H^0}{R}$, and the intercept with the *y* axis, corresponding to $\ln(A)$, allow determining the initial guesses for the nonisothermal regression as reported in Table 3.

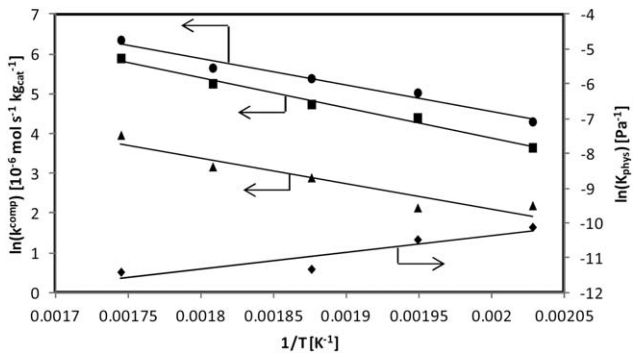

Figure 9. Arrhenius plot, $\ln(k^{comp})$ and $\ln(K_{phys})$ as function of the reciprocal of temperature for which k^{comp} and K_{phys} are obtained from Table 2.

Nonisothermal regression

Starting from the initial estimates reported in Table 3, the values of the kinetic and equilibrium coefficients at the mean temperature equal to 531.48 K, and activation energies and physisorption enthalpy were estimated via nonisothermal regression with simultaneously considering all data that have been measured as reported in Table 4.

Table 3. Determined Values of the Pre-Exponential Factor, Kinetic/Equilibrium Coefficient at Mean Temperature, that is, 531.48 K, and Activation Energy and Reaction Enthalpy by the Isothermal Regression and the Arrhenius Plot, See Figure 9

	A (mol s^{-1} kg^{-1}_{cat} or 10^{-9} Pa^{-1})	k_{Tm} or K_{Tm} (10^{-6} mol s^{-1} kg^{-1}_{cat} or 10^{-5} Pa^{-1})	E_a or ΔH^0 (kJ mol^{-1})
$k^{comp}_{PCP(1)}$	59.1	206.6	55.5
$k^{comp}_{PCP(2)}$	116.5	118.4	62.8
k^{comp}_{cr}	2.8	17.5	53.0
K_{phys}	2.0	1.8	−40.0

Table 4. Parameter Estimates, Corresponding Approximate 95% Individual Confidence Interval and *t* Values of the Kinetic/Equilibrium Coefficients at Mean Temperature and Activation Energies and Reaction Enthalpy Determined by Nonisothermal Regression to the Experimental Data, See Table 6 (Supporting Information), of the Kinetic Model Given by the Set of Eqs. 3–5, in Which the Net Rates of Formation are Given by Eqs. 17–19

	$k^{comp}_{T_m}$ or K_{T_m} (10^{-6} mol s^{-1} kg^{-1}_{cat} or 10^{-5} Pa^{-1})	|t Value| Tabulated Value: 2.0	E^{comp}_a or ΔH (kJ mol^{-1})	|t Value| Tabulated Value: 2.0
$k^{comp}_{PCP(1)}$	200.0 ± 22.8	18.5	53.5 ± 7.1	15.9
$k^{comp}_{PCP(2)}$	114.5 ± 13.7	17.6	61.4 ± 7.8	16.6
k^{comp}_{cr}	14.6 ± 2.4	12.7	68.0 ± 9.7	14.8
K_{phys}	1.0 ± 0.6	3.3	-88.6 ± 28.0	6.8

Table 5. Binary Correlation Coefficient Matrix as Determined by Nonisothermal Regression to the Experimental Data, See Table 6 (Supporting Information), of the Kinetic Model Given by the Set of Eqs. 3–5, in Which the Net Rates of Formation are Given by Eqs. 17–19

	$k^{comp}_{T_m,PCP(1)}$	$k^{comp}_{T_m,PCP(2)}$	$k^{comp}_{T_m,cr}$	$K_{T_m,phys}$	$E^{comp}_{a,PCP(1)}$	$E^{comp}_{a,PCP(2)}$	$E^{comp}_{a,cr}$	ΔH_{phys}
$k^{comp}_{T_m,PCP(1)}$	1.00	0.92	0.60	0.90	−0.72	−0.62	−0.41	0.36
$k^{comp}_{T_m,PCP(2)}$	0.92	1.00	0.57	0.85	−0.65	−0.72	−0.39	0.34
$k^{comp}_{T_m,cr}$	0.60	0.57	1.00	0.63	−0.36	−0.33	−0.92	0.40
$K_{T_m,phys}$	0.90	0.85	0.63	1.00	−0.54	−0.49	−0.39	0.65
$E^{comp}_{a,PCP(1)}$	−0.72	−0.65	−0.36	−0.54	1.00	0.87	0.26	0.18
$E^{comp}_{a,PCP(2)}$	−0.62	−0.72	−0.33	−0.49	0.87	1.00	0.26	0.17
$E^{comp}_{a,cr}$	−0.41	−0.39	−0.92	−0.39	0.26	0.26	1.00	−0.18
ΔH_{phys}	0.36	0.34	0.40	0.65	0.18	0.17	−0.18	1.00

The model has a higher F value for the global significance of the model, 2365, than the corresponding tabulated F value, 3.9. All parameters are estimated significantly, as reflected by their confidence interval and corresponding t value exceeding the tabulated t value. The coefficients concerning cracking, k^{comp}_{cr}, and physisorption, K_{phys}, have the widest confidence intervals. As discussed in Isothermal Regression section, the information with respect to k^{comp}_{cr} is contained in the data acquired at higher temperatures whereas the information with respect to K_{phys} is contained in the data acquired at lower temperature. Literature values for the activation energies of PCP-branching and cracking are difficult to find due to their composite nature. However, the physisorption enthalpy estimated, 88 kJ mol^{-1}, corresponds rather well to physisorption studies of *n*-hexane on ZSM-5, that is, 70–80 kJ mol^{-1}.[19,51,52] A different activation energy for PCP-branching to 2MP and 3MP was obtained, resp. 53 and 61 kJ mol^{-1}. This composite activation energy comprises the physisorption enthalpy, the dehydrogenation enthalpy, the protonation enthalpy, the activation energy of the elementary step. The physisorption enthalpy is estimated to be about −90 kJ mol^{-1}, the dehydrogenation enthalpy is determined by thermodynamic calculations to be about 100 kJ mol^{-1} and protonation enthalpies are reported to be within the range of about −70 to −90 kJ mol^{-1}.[19,25] The activation energy for PCP-branching (s,s) is reported to be equal to about 110–130 kJ mol^{-1}.[19,25] From the parameter estimated, the activation energy for PCP-branching (s,s) amounts to 120–140 kJ mol^{-1} which corresponds rather well to the literature values. The occurrence of diffusion effects is not pronounced as this would lead to an observed activation energy which is much smaller.[1] The activation energy for cracking is estimated to be the highest, that is, 68 kJ mol^{-1}, as expected since propane is a secondary product and is only formed in the higher temperature range.

The F value for the model adequacy was determined at 1.75 which slightly exceeds the tabulated value at 95% significance with resp. 67 and 33 degrees of freedom, that is, 1.69. This means that, statistically, the model is found to be marginally inadequate. Some deviations between the model calculated and observed values are present which cannot be solely attributed to experimental errors. As stated in Model and Parameter Estimates Assessment section, the test for the model adequacy is a quite severe test. It can, hence, be

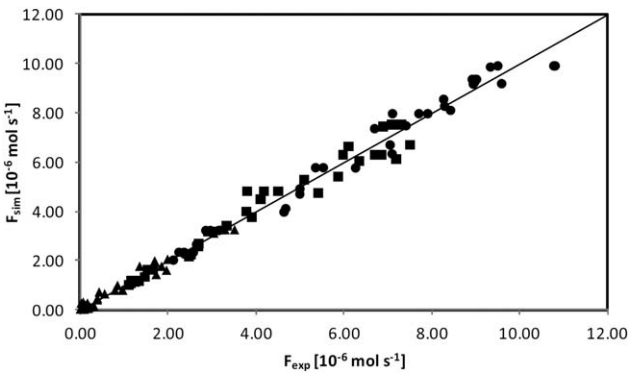

Figure 10. Parity diagram for the molar outlet flow rate of 2MP (filled circle), 3MP (filled square) and propane (filled triangle) determined by solving the set of Eqs. 3–5, in which the net rates of formation are given by Eqs. 17–19 using the parameters from Table 4.

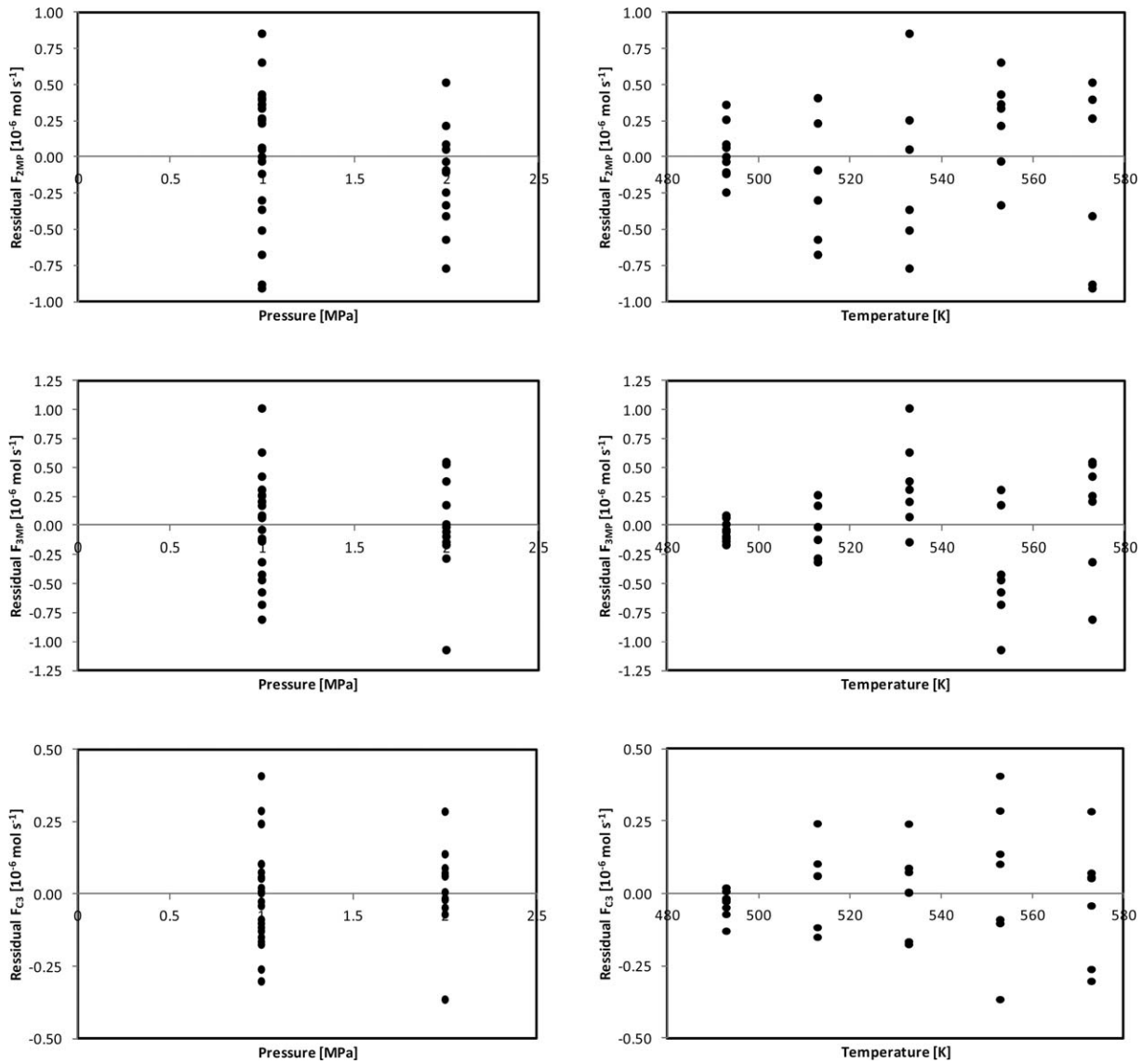

Figure 11. Residual figures for the molar outlet flow rate of 2MP (top), 3MP (middle) and propane (bottom) as function of pressure (left) and temperature (right) determined by solving the set of Eqs. 3–5, in which the net rates of formation are given by Eqs. 17–19 using the parameters from Table 4.

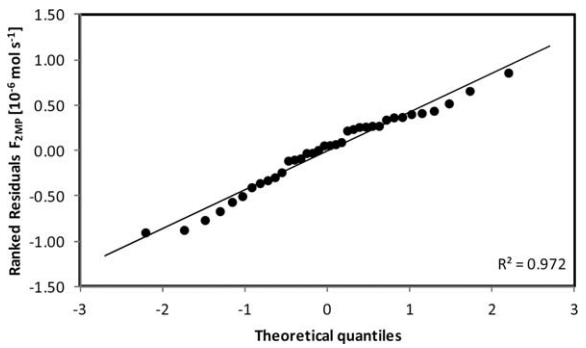

Figure 12. Normal probability figure for the molar outlet flow rate of 2MP determined by solving the set of Eqs. 3–5, in which the net rates of formation are given by Eqs. 17–19 using the parameters from Table 4.

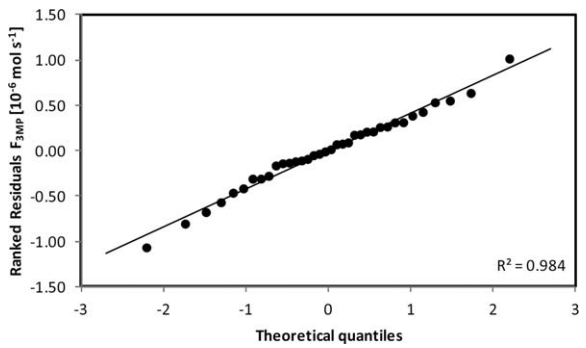

Figure 13. Normal probability figure for the molar outlet flow rate of 3MP determined by solving the set of Eqs. 3–5, in which the net rates of formation are given by Eqs. 17–19 using the parameters from Table 4.

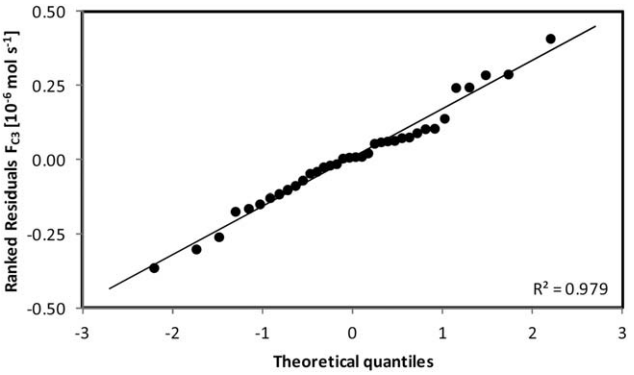

Figure 14. Normal probability figure for the molar outlet flow rate of propane determined by solving the set of Eqs. 3–5, in which the net rates of formation are given by Eqs. 17–19 using the parameters from Table 4.

concluded that the model performs quite fair within the investigated range of operating conditions but that extrapolations should be approached with sufficient care.

Table 5 shows the binary correlation coefficient matrix obtained from the nonisothermal regression. No binary correlation coefficients higher than 0.95 are obtained and, hence, the kinetic parameters can be considered to be uncorrelated. A maximum binary correlation coefficient of 0.92 occurs obtained between $k^{\text{comp}}_{\text{Tm,PCP(1)}}$ and $k^{comp}_{Tm,\text{PCP(2)}}$. Both parameters are closely related as both represent the simultaneous formation of an isomerization product from *n*-hexane.

Model performance

An initial visual assessment of the model's performance can be made from Figures 3 and 4. It is clear that the model is able to simulate the observed trends very well. In Figure 10, the parity diagram of the three responses, that is, the three reaction products: 2MP, 3MP, and propane, are shown. For all three components, the simulated points are distributed uniformly around the first bisector of the parity diagram, indicating that no pronounced systematic deviations occur between model simulations and experimental data. For the propane response, however, at low outlet flow rates, which are corresponding to the experiments at lowest temperatures, the largest relative deviations are obtained which is agreement with the wider confidence intervals of estimates for the cracking rate coefficients at these temperatures, as discussed in Isothermal Regression section.

The behavior of the responses' residuals which are expected to approach the true experimental error does also not exhibit any particular trend with the operating conditions, that is, temperature and pressure, as shown by the residual figures, see Figure 11. For all responses and operating conditions, the residuals are normally distributed around the x axis indicating no lack of fit by the model and the normal distribution of the experimental error with expected value equal to zero. However, based on the experimental error determined by repeat experiments, the variance is slightly higher than expected as indicated by the F value for the model adequacy.

Figures 12–14 show the normal probability figures for each response. For all three responses, the linear regression of the ranked residuals to the theoretical quantiles leads to a R^2-value exceeding 0.97. Also a visual inspection of the normal probability figures show that the experimental error is distributed normally.

Conclusions

A systematic methodology for the kinetic modeling of chemical reactions has been proposed. The main goal is to find an optimal balance between statistical significance and physical meaning. The number of elementary steps that occurs will, in general, exceed by far the number of parameters that can be statistically significantly determined. First, the experimental data should be examined to provide qualitative insights in the underlying mechanism of the investigated reaction. This understanding can subsequently be translated into rate-equations describing these reaction mechanisms. Transforming the rate equations into equations linear in the parameters, for example, via isothermal regression, provides a relatively easy and straightforward manner to obtain good initial parameters values for the simultaneous, nonisothermal determination of the kinetic parameters. The estimates resulting from the regression should both have a sound physical meaning as well as be statistically significant. Other statistical tools, such as the binary correlation coefficient matrix, can be used to elucidate the underlying kinetics, that is, how steps potentially compensate for each other. Additionally, the binary correlation coefficient matrix can reveal the relationship between the mathematics describing the reaction mechanism and the corresponding physics. Residual analysis, consisting of parity diagrams and residual, performance and normal probability figures, indicate the model adequacy and distribution of the experimental error.

The developed methodology was successfully applied to *n*-hexane hydroisomerization over a bifunctional catalyst, that is, Pt/H-ZSM-5. The kinetic model obtained was able to describe the experimental data very satisfactory. However, the variance of the residuals could not only be attributed to experimental error as repeat experiments and the test for model adequacy have revealed. All parameter estimates obtained could be traced back in terms of the phenomena that were actually occurring. The values of the composite activation energies for PCP-branching and β-scission were determined to be statistically significant. The composite activation energy for β-scission was higher than those of PCP-branching, hence, the production of cracked products, that is, propane, is regarded as a secondary reaction which is only becoming important at higher temperatures, as experimentally observed. The composite activation energy for PCP-branching toward 3MP exceeds that of the reaction leading to 2MP, which resulted from the experimental observation that the 2MP to 3MP molar ratio decreases with increasing temperature. This could be due to intracrystalline diffusion effects in the medium pore sized MFI support. This support is selective to the formation of 2MP at lower conversions. The physisorption enthalpy for the C_6 components corresponds well with reported values from literature.

Acknowledgments

This article reports work undertaken in the context of the project "OCMOL, Oxidative Coupling of Methane followed by Oligomerization to Liquids". OCMOL is a Large Scale Collaborative Project supported by the European

Commission in the 7th Framework Programme (GA n°228953). For further information about OCMOL see: http://www.ocmol.eu or http://www.ocmol.com. This work was supported by the "Long Term Structural Methusalem Funding by the Flemish Government."

Notation

Roman symbols

2MP = 2-methyl-pentane
3MP = 3-methyl-pentane
$a_{C,j}$ = the number of carbon atoms in component j,
A = pre-exponential factor in the nth reaction order, (mol $kg_{cat}^{-1})^{n-1}s^{-1}$
$\underline{b}$ = estimated parameter vector
C_3 = propane
C_j = molar concentration of component j, mol m^{-3}
C_{H^+} = acid site concentration, mol kg_{cat}^{-1}
d.f. = degrees of freedom
E_a = activation energy, J mol^{-1}
F_a = F value for adequacy
F_j = molar flow rate of component j, mol s^{-1}
F_s = F value for significance
ΔH^0 = standard enthalpy, J mol^{-1}
H_2 = hydrogen
i = counter
j = counter
k = reaction rate coefficient in the nth reaction order, ((mol $kg_{cat}^{-1})^{n-1}s^{-1}$)
K = equilibrium coefficient, Pa^{-1}
nC$_6$ = n-hexane
$n_e(j)$ = number of repeat experiments at the jth set of repeat experiments
n_{exp} = number of experiments
n_{par} = number of parameters
n_{resp} = number of responses
p_j = partial pressure of component j, Pa
r = reaction rate, mol s^{-1} kg_{cat}^{-1}
R_j = net rate of formation of component j, mol s^{-1} kg_{cat}^{-1}
R = universal gas constant, J mol^{-1} K^{-1}
$s(b_j)$ = standard deviation of parameter j
S_j = selectivity for component j, mol s^{-1}, (mol $s^{-1})^{-1}$
$t(b_j)$ = t-value for parameter j
T = temperature, K
T_m = mean temperature, K
$V(b)$ = variance-covariance matrix
V_p = pore volume, m^3 kg_{cat}^{-1}
$w_{i,j}$ = statistical weight of response i and experiment j
W = catalyst mass, kg_{cat}
X_j = conversion of component j, mol s^{-1}, (mol $s^{-1})^{-1}$
$y_{i,j}$ = observed value for response i at experiment j, variable

Greek symbols

β = real parameter vector
$\rho_{i,j}$ = binary correlation between parameters i and j

Subscripts

cr = cracking
deh = dehydrogenation
LOF = lack-of-fit
pcp = PCP-branching
PE = pure error
phys = physisorption
pr = protonation
REG = regression
RES = residual
tot = total
+ = carbenium ion
= = alkene
exp = experimental
phys = physisorption
sim = simulated
^ = calculated

Superscripts

0 = inlet
comp = composite

Literature Cited

1. Froment GF, Bischoff KB, De Wilde J. *Chemical Reactor Analysis and Design*, *3rd ed*. New York: Wiley, 2010.
2. Marin GB, Yablonsky GS. *Kinetics of Chemical Reactions: Decoding Complexity*. New York: Wiley, 2011.
3. Kittrell JR. Mathematical modeling of chemical reactions. *Adv Chem Eng*. 1970;8:97–183.
4. Dumesic JA, Rudd DF, Aparicio LM, Rekiske JE, Trevine AA. *The Microkinetics of Heterogeneous Catalysis*. Washington, DC: American Chemical Society, 1993.
5. Thybaut JW, Marin GB. Testing of catalytic properties. In: Centi G, editor. *Catalysis, Encyclopedia of Life Support Systems (EOLSS)*, Developed under the Auspices of the UNESCO. Oxford: Eolss Publishers, 2009.
6. Thybaut JW, Marin GB. Kinetics of catalyzed reactions—heterogeneous. In: Horvath I, editor. *Encyclopedia of Catalysis*. New York: Wiley, 2010.
7. Berger RJ, Stitt EH, Marin GB, Kapteijn F, Moulijn JA. Eurokin—chemical reaction kinetics in practice. *Cattech*. 2001;5:30–60.
8. Artetxe M, Lopez G, Amutio M, Bilbao J, Olazar M. Kinetic modelling of the cracking of HDPE pyrolysis volatiles on a HZSM-5 zeolite based catalyst. *Chem Eng Sci*. 2014;116:635–644.
9. Devoldere KR, Froment GF. Coke formation and gasification in the catalytic dehydrogenation of ethylbenzene. *Ind Eng Chem Res*. 1999; 38:2626–2633.
10. Froment GF. Kinetic modeling of hydrocarbon processing and the effect of catalyst deactivation by coke formation. *Catal Rev Sci Eng*. 2008;50:1–18.
11. Froment GF. Fundamental kinetic modeling of catalytic hydrocarbon conversion processes. *Rev Chem Eng*. 2013;29:385–412.
12. Mier D, Gayubo AG, Aguayo AT, Olazar M, Bilbao J. Olefin production by cofeeding methanol and n-butane: kinetic modeling considering the deactivation of HZSM-5 zeolite. *AIchE J*. 2011;57: 2841–2853.
13. Allain JF, Magnoux P, Schulz P, Guisnet M. Hydroisomerization of n-hexane over platinum mazzite and platinum mordenite catalysts—kinetics and mechanism. *Appl Catal A*. 1997;152:221–235.
14. Baltanas MA, Froment GF. Computer-generation of reaction networks and calculation of product distributions in the hydroisomerization and hydrocracking of paraffins on Pt-containing bifunctional catalysts. *Comput Chem Eng*. 1985;9:71–81.
15. Baltanas MA, Vansina H, Froment GF. Hydroisomerization and hydrocracking. 5. Kinetic-analysis of rate data for n-octane. *Ind Eng Chem Prod Res Dev*. 1983;22:531–539.
16. Martens GG, Thybaut JW, Marin GB. Single-event rate parameters for the hydrocracking of cycloalkanes on Pt/US-Y zeolites. *Ind Eng Chem Res*. 2001;40:1832–1844.
17. Steijns M, Froment G, Jacobs P, Uytterhoeven J, Weitkamp J. Hydroisomerization and hydrocracking. 2. Product distributions from normal-decane and normal-dodecane. *Ind Eng Chem Prod Res Dev*. 1981;20:654–660.
18. Steijns M, Froment GF. Hydroisomerization and hydrocracking. 3. Kinetic-analysis of rate data for normal-decane and normal-dodecane. *Ind Eng Chem Prod Res Dev*. 1981;20:660–668.
19. van de Runstraat A, van Grondelle J, van Santen RA. Microkinetics modeling of the hydroisomerization of n-hexane. *Ind Eng Chem Res*. 1997;36:3116–3125.
20. Raghuveer CS, Thybaut JW, De Bruycker R, Metaxas K, Bera T, Marin GB. Pyridine hydrodenitrogenation over industrial NiMo/Î[3]-Al2O3 catalyst: application of gas phase kinetic models to liquid phase reactions. *Fuel*. 2014;125:206–218.
21. Thybaut JW, Narasimhan CSL, Denayer JF, Baron GV, Jacobs PA, Martens JA, Marin GB. Acid-metal balance of a hydrocracking catalyst: ideal versus nonideal behavior. *Ind Eng Chem Res*. 2005;44: 5159–5169.
22. Thybaut JW, Narasimhan CSL, Marin GB. Bridging the gap between liquid and vapor phase hydrocracking. *Catal Today*. 2006;111:94–102.
23. Vansina H, Baltanas MA, Froment GF. Hydroisomerization and hydrocracking. 4. Product distribution from n-octane and 2,2,4-trimethylpentane. *Ind Eng Chem Prod Res Dev*. 1983;22:526–531.

24. Weitkamp J. Hydrocracking, cracking and isomerization of hydrocarbons. *Erdol Kohle Erdgas Petrochemie*. 1978;31:13–22.
25. Vandegehuchte BD, Thybaut JW, Martinez A, Arribas MA, Marin GB. *n*-Hexadecane hydrocracking single-event microkinetics on Pt/H-beta. *Appl Catal A*. 2012;441–442:10–20.
26. Robson H. *Verified Synthesis of Zeolitic Materials*. Amsterdam: Elsevier, 2001.
27. EUROKIN_fixed-bed_html, EUROKIN spreadsheet on requirements for measurement of intrinsic kinetics in the gas-solid fixed-bed reactor, 2012.
28. Berty JM. Reactor for vapor-phase catalytic studies. *Chem Eng Prog*. 1974;70:78–85.
29. Athena Visual Studio, Available at http://www.athenavisual.com/. Last accessed on May 10, 2014.
30. Stewart WE, Caracotsios M. *Computer-Aided Modeling of Reactive Systems*. New York: Wiley, 2008.
31. Bard Y. *Nonlinear Parameter Estimation*. Waltham: Academic Press, 1974.
32. Froment GF, Hosten LH. Catalytic kinetics: modeling. In: Anderson J, Boudart M, editors. *Catalysis Science and Technology*. London: Royal Society of Chemistry, 1981.
33. Edgar TF, Himmelblau DM, Lasdon L. *Optimization of Chemical Processes*. Ontario: McGraw-Hill Higher Education, 2001.
34. Box GEP, Draper NR. Bayesian estimation of common parameters from several responses. *Biometrika*. 1965;52:355–365.
35. Box MJ, Draper NR. Estimation and design for multiresponse nonlinear models, nonhomogenous variance structure. *Ann Math Stat*. 1970;41:1391.
36. Box MJ, Draper NR, Hunter WG. Missing values in multiresponse nonlinear model fitting. *Technometrics*. 1970;12:613–620.
37. Buzzi-Ferraris G. Planning of experiments and kinetic analysis. *Catal Today*. 1999;52:125–132.
38. Buzzi-Ferraris G, Manenti F. Kinetic models analysis. *Chem Eng Sci*. 2009;64:1061–1074.
39. Buzzi-Ferraris G, Manenti F. Better reformulation of kinetic models. *Comput Chem Eng*. 2010;34:1904–1906.
40. BzzMath: Numerical libraries in C++, Available at http://www.chem.polimi.it/homes/gbuzzi. Last accessed on May 10, 2014.
41. Buzzi-Ferraris G, Manenti F. BzzMath: Library Overview and Recent Advances in Numerical Methods. In: 22 European Symposium on Computer Aided Process Engineering: London, UK, Vol. 30, 2012:1312–1316.
42. Boudart M. Physical limitations to values of parameters used in rate equations for reactions catalyzed by solids. *Industrie Chimique Belge-Belgische Chemische Industrie*. 1966;31:74.
43. Kittrell JR, Mezaki R. Discrimination among rival Hougen-Watson models through intrinsic parameters. *AIchE J*. 1967;13:389–392.
44. Epelde E, Aguayo AT, Olazar M, Bilbao J, Gayubo AG. Kinetic model for the transformation of 1-butene on a K-modified HZSM-5 catalyst. *Ind Eng Chem Res*. 2014;53:10599–10607.
45. Froment GF. Kinetic modeling of acid-catalyzed oil refining processes. *Catal Today*. 1999;52:153–163.
46. Rosenbrock HH. An automatic method for finding the greatest or least value of a function. *Comput J*. 1960;3:175–184.
47. Marquardt DW. An algorithm for least-squares estimation of nonlinear parameters. *J Soc Ind Appl Math*. 1963;11:431–441.
48. Choudhary VR, Akolekar DB. Shuttlecock-shuttlebox model for shape selectivity of medium-pore zeolites in sorption and diffusion. *J Catal*. 1989;117:542–548.
49. Ferreira AFP, Mittelmeijer-Hazeleger MC, Bergh JVD, Aguado S, Jansen JC, Rothenberg G, Rodrigues AE, Kapteijn F. Adsorption of hexane isomers on MFI type zeolites at ambient temperature: understanding the aluminium content effect. *Microporous Mesoporous Mater*. 2013;170:26–35.
50. Thybaut JW, Marin GB, Baron GV, Jacobs PA, Martens JA. Alkene protonation enthalpy determination from fundamental kinetic modeling of alkane hydroconversion on Pt/H-(US)Y-zeolite. *J Catal*. 2001;202:324–339.
51. Makowski W, Majda D. Equilibrated thermodesorption studies of adsorption of *n*-hexane and *n*-heptane on zeolites Y, ZSM-5 and ZSM-11. *Appl Surf Sci*. 2005;252:707–715.
52. Savitz S, Myers AL, Gorte RJ, White D. Does the cal-ad method distinguish differences in the acid sites of H-MFI? *J Am Chem Soc*. 1998;120:5701–5703.

Manuscript received May 28, 2014, and revision received Sep. 22, 2014.